

Case Study on the Correlation between Crystal Packing and Miscibility of Chlorinated Thiophene–Based Donor Polymers for Nonfullerene Organic Solar Cells with Long Shelf Life

Sung Jae Jeon, Yong Woon Han, Young Hoon Kim, and Doo Kyung Moon*

Nonfullerene organic solar cells (NFOSCs) have proven to have greater potential in terms of efficiency than fullerene-based OSCs. However, the heterogeneity of nonfullerene acceptors (NFAs)-based blend morphology is complex, making it difficult to understand, especially as its optimization requires that compatibility among the molecules be considered. Herein, P(Cl)($F=0.5$) is newly synthesized with a type of terpolymer to increase compatibility with NFAs relative to that of conventional polymers. As a result, the combination of P(Cl)($F=0.5$) with IDIC increases its power conversion efficiency (PCE) to 12.1%, compared with that of P(Cl):ITIC-Th and P(F-Cl):IT-4F. However, during the shelf life stability of optimized devices without encapsulation, a rapid decrease in the efficiency of P(Cl)($F=0.5$):IDIC and P(F-Cl):IT-4F is observed; the PCEs of P(Cl)($F=0.5$):IDIC and P(F-Cl):IT-4F decrease to 24.1% and 43.5% of their initial values for up to 350 and 398 h, respectively. On the contrary, P(Cl):ITIC-Th exhibits superior longterm air stability with a PCE decrease of -2% (for 317-h) and 9% (for 2002-h) compared with the initial PCE. To understand this phenomenon, the correlation between crystallinity and miscibility of blend films is systematically investigated. In short, the balanced crystallinity and miscibility of donor and acceptor induces a relatively more stable morphology.


1. Introduction

In regard to conjugated polymers, solution-processed organic solar cells (OSCs) have drawn immense attention due to their low cost, mechanical flexibility, light weight, and transparency in portable organic electronics.^[1,2] State-of-the-art OSCs have achieved power conversion efficiencies (PCEs) of over 16%^[3–5] and 17%^[6] in single solar cells and tandem solar cells, respectively, due to the development of nonfullerene

acceptors (NFAs).^[7–9] This progress has resulted in the near commercialization of OSCs. However, despite this achievement, problems such as the high cost of raw materials and device fabrication persist.^[10,11] In particular, the high cost of conjugated polymers is an obstruction to the development of OSCs.^[12] To solve this problem, a simple design strategy of wide-bandgap donor polymers based on 2D benzo[1,2-b:4,5-b']dithiophene (2DBDT) and halogenated heterocycle rings, which are relatively inexpensive, is proposed.^[13,14] In our previous study, a low-cost and high-performance wide-bandgap donor polymer, P(Cl), was developed using a 3-chlorothiophene unit in the 2DBDT polymer backbone. Based on theoretical calculations, this polymer was expected to perform relatively better upon the introduction of chlorine (Cl) compared with that of fluoro (F), depending on the depth of its highest-occupied molecular orbital (HOMO) level and the strength of its dipole moment. As a result, the 3,9-bis(2-methylene-(3-(1,1-dicyanomethylene)11,

11-tetrakis(4-hexylthienyl)-thiethieno[2,3-d:2',3'-d']-s-indaceno[1,2-b:4,5-b']dithiophene (ITIC-Th)-blended P(Cl) showed a high PCE of 11.4% with low synthetic complexity compared with the commercialized polymers.^[14] Most recently, P(F-Cl) was synthesized to obtain more efficient OSCs by introducing fluoro-substituted 2DBDT (F-2DBDT) instead of the nonhalogenated 2DBDT of P(Cl). The polymer was expected to reveal F and Cl effects simultaneously by aligning its frontier energy levels closer to NFAs. Thus, the optimized device of P(F-Cl) with 3,9-bis(2-methylene-((3-(1,1-dicyanomethylene)-6,7-difluoro)-indanone))-5,5,11,11-tetrakis(4-hexylphenyl)-dithieno[2,3-d:2',3'-d']-s-indaceno[1,2-b:5,6-b']dithiophene (IT-4F) showed a higher PCE (11.8%) compared with that of P(Cl):ITIC-Th. However, this device exhibited poor morphology and low reliability, due to the high level of aggregation and low solubility.^[15] This way, the photovoltaic performance was closely related to the film morphology; thus, compatibility between the components of the photoactive layer should be controlled carefully.^[16] Generally, extremely low miscibility between the donor and acceptor materials may result in oversized domains,

Dr. S. J. Jeon, Dr. Y. W. Han, Y. H. Kim, Prof. D. K. Moon
Nano and Information Materials (NIMs) Laboratory, Department of
Chemical Engineering
Konkuk University
120, Neungdong-ro, Gwangjin-gu, Seoul 05029, Korea
E-mail: dkmoon@konkuk.ac.kr

 The ORCID identification number(s) for the author(s) of this article can be found under <https://doi.org/10.1002/solr.202000074>.

DOI: 10.1002/solr.202000074

thus reducing the efficiency level of charge separation and charge transport percolating pathways. On the contrary, extremely high miscibility may lead to excessively mixed amorphous domains, thus increasing the unfavorable bimolecular recombination.^[7,16–22]

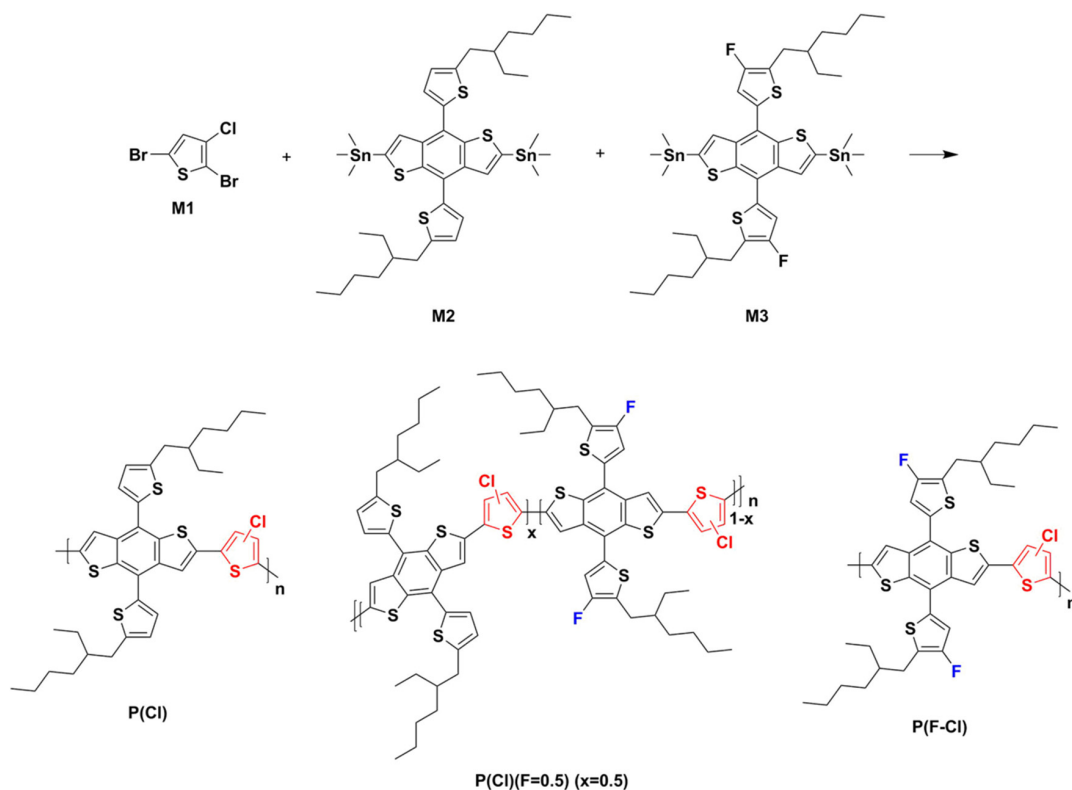
In this study, a new chlorinated thiophene-based donor polymer P(Cl)(*F* = 0.5) was designed and synthesized with a type of terpolymer to enhance its compatibility with relative NFAs. P(Cl)(*F* = 0.5) was successfully developed by introducing F-2DBDT and 2DBDT as the donor units at mole ratios of 0.5:0.5 in the polymerization process, respectively. The optical and electrochemical properties of P(Cl)(*F* = 0.5) were analyzed and compared with those of the donor polymers of P(Cl), and P(F-Cl) and various low-bandgap NFAs, such as ITIC-Th, 2,2'-(2*Z*,2'*Z*')-((4,4,9,9-tetrahexyl-4,9-dihydro-*s*-indaceno[1,2*b*:5,6-*b*']dithiophene-2,7-diyl)bis(methanylylidene))bis(3-oxo-2,3-dihydro-1*H*-indene-2,1-diylidene)dimalononitrile (IDIC) and IT-4F. Based on the results obtained, the photovoltaic devices of P(Cl)(*F* = 0.5) that were fabricated and optimized with IDIC exhibited the best PCE, 12.1% (certified PCE is 12.48% from the Nano Convergence Practical Application Center [NCPAC] in Korea), among the donor polymers. These results were consistent with the data on photoluminescence, charge carrier mobility, and morphology analysis of optimized devices. Further studies on the shelf life stability of the optimized devices showed a slight decrease in the efficiency of all devices (3.0–8.0% over 400 h) compared with each initial PCE under encapsulation, whereas, devices made of P(Cl)(*F* = 0.5):IDIC and P(F-Cl):IT-4F

without encapsulation exhibited poor air stability compared with P(Cl):ITIC-Th. To identify the cause of this phenomenon, the correlation between crystallinity and miscibility in each film was systematically investigated through grazing-incidence wide-angle X-ray scattering (GIWAXS), contact angles, and differential scanning calorimetry (DSC). Consequently, in blending donor polymers and NFAs, if the values of crystals indicating face-on-to-edge-on structure crystals and the molecular interactions are too large or too small, the consequent excessive aggregation or mixing over time may decrease the stability of the devices. This indicates acceleration of phase separation between the donor polymers and the NFAs due to a great imbalance between crystallinity and miscibility, compared with initial blend films. As a result, this study will emphasize the importance of correlations between the crystallinity and miscibility of donor polymers and NFAs for highly efficient NFOSCs.

2. Results and Discussion

2.1. Material Design, Theoretical Calculations, and Physical Properties

Three chlorinated thiophene-based donor polymers for P(Cl), P(Cl)(*F* = 0.5), and P(F-Cl) are shown in **Scheme 1**. P(Cl) and P(F-Cl) were already characterized and reported in the previous study.^[14,15] P(Cl)(*F* = 0.5) was newly designed and synthesized with a type of copolymer to enhance compatibility with the



Scheme 1. Synthesis routes for P(Cl), P(Cl)(*F* = 0.5), and P(F-Cl).

diverse and high-performance NFAs. The terpolymer was successfully developed by introducing F-2DBDT and 2DBDT as the donor units at mole ratios of 0.5:0.5 in the polymerization process, respectively (Figure S1, Supporting Information). The theoretical and physical properties of the synthesized donor terpolymer, P(Cl)(F = 0.5), were closely analyzed and compared with P(Cl) and P(F-Cl). First, the density functional theory (DFT) calculations for the designed donor polymers of P(Cl), P(Cl)(F = 0.5), and P(F-Cl) were carried out in repeating units (n) which was equivalent to 2 ($n = 2$). As shown in Figure S2, Supporting Information, the HOMO levels were down-shifted and the bandgaps tended to decrease with increasing F-2DBDT units in the chlorinated thiophene-based polymer backbones. This was because the F-2DBDT unit which had two F atoms had a higher oxidation stability than the 2DBDT unit.^[23,24] In addition, as shown in Scheme S1, Supporting Information, because the number of F-2DBDT units in the polymer backbones was increased, and the curvatures of model compounds based on the observations that θ_1 , θ_2 , and θ_3 were tilted in the positive direction and their sum decreased, P(F-Cl) was expected to have the highest planarity, P(Cl)(F = 0.5) medium planarity, and P(Cl) the lowest planarity. Details of the calculated results are shown in Table S1, Supporting Information. The new polymer, P(Cl)(F = 0.5), showed the fine solubility dissolving effectively in common organic solvents such as chloroform, chlorobenzene, and *o*-dichlorobenzene in spite of introducing a more rigid F-2DBDT than 2DBDT in the polymer backbone.^[13,25] As a result of the measurement of gel permeation chromatography (GPC), all three polymers yielded relatively high average molecular weights ($M_n \geq 25$ kDa).^[14,22] The results of thermogravimetric analysis (TGA) confirmed that the temperature at 5% weight loss (T_d) decreased in the order of P(Cl), P(Cl)(F = 0.5), and P(F-Cl) (Figure S3, Supporting Information). This was contrary to the common tendency of polymers where thermal stability increases due to the introduction of F.^[24] This tendency is caused by the fact that solubility is decreased to obtain a low molecular weight as the F-2DBDT units are introduced into the polymer backbones. In addition, from the analysis results of the crystalline natures of donor polymers taken from DSC, no peaks showing differences in crystallinity were observed at 30–270 °C (Figure S4, Supporting Information). The details of the measured results are shown in Table 1.

2.2. Optical and Electrochemical Properties

The optical and electrochemical properties of P(Cl)(F = 0.5) were investigated through ultraviolet–vis spectroscopy (UV) and cyclic

Table 1. Physical and thermal properties of donor polymers.

| Polymer | Yield [%] | M_n^a [kDa] | M_w^a [kDa] | PDI ^{a)} | T_d^b [°C] |
|----------------|-----------|---------------|---------------|-------------------|--------------|
| P(Cl) | 90.0 | 38.1 | 82.5 | 2.17 | 350 |
| P(Cl)(F = 0.5) | 85.0 | 29.7 | 68.1 | 2.30 | 345 |
| P(F-Cl) | 77.0 | 25.1 | 38.8 | 1.55 | 330 |

^{a)}The parameters (M_n : number-average molecular weight, M_w : weight-average molecular weights, PDI: polydispersity index) determined by GPC in chloroform using polystyrene standards; ^{b)}Temperature resulting in a 5% weight loss.

voltammetry (CV) in Figure 1. To profoundly understand the optical and electrochemical interactions between the donor and acceptor, P(Cl), P(F-Cl), and NFAs (ITIC-Th, IDIC, and IT-4F) were also analyzed. The donor polymers showed two absorption bands in the solution and film states at both the 300–400 and 400–600 nm regions, according to the π – π^* transition intramolecular charge transfer (ICT) between the donor and chlorinated thiophene units of the donor polymers, whereas strong ICT effects in NFAs showed the clear vibronic band in the 600–800 nm region.^[13,14] Therefore, complementary optical absorption could be expected in blended donor polymers and NFAs. After measuring the UV wavelength in the chloroform solution states with different concentrations in the order of 10^{-5} M (Figure S5, Supporting Information), the results obtained were substituted into the Beer–Lambert equation.^[13,14,22] As shown in Figure 1a, the average molar absorption coefficients (ϵ) of the donor polymers and NFAs were calculated. In particular, ϵ for donor polymers increased in the order of P(Cl), P(Cl)(F = 0.5), and P(F-Cl). This is because the electronegativity and dipole moment effects increase as the F-2DBDT units are introduced into the polymer backbones.^[13,23] On the other hand, ϵ of NFAs yielded similar values, ≈ 11.0 – 12.7×10^4 M⁻¹ cm⁻¹.^[23] As shown in Figure 1b, the wavelengths of all of the materials were red-shifted to the long-wavelength region as the materials transitioned from the solution to film state, due to the reduction in the distance between molecules and the increase in aggregation effects.^[13,14] In particular, in the case of donor polymers, as F-2DBDT was introduced in polymer backbones instead of 2DBDT, the shoulder peaks, which indicate π – π stacking effects, were observed to decrease. The tendency was the highest in P(Cl)(F = 0.5) because the structural complexity and regiorandom segments of P(Cl)(F = 0.5) increased as its polymer chains grew into a terpolymer, thus interrupting the high stacking of molecular structures.^[26,27] This tendency was also observed in the optical bandgaps (E_g^{opt}). A relatively lower bandgap of 1.97 eV was observed for P(Cl), but relatively higher bandgaps of 2.01 and 1.99 eV were observed for P(Cl)(F = 0.5) and P(F-Cl), respectively. Finally, the electrochemical properties of donor polymers and NFAs were analyzed through CV measurements (Figure S6, Supporting Information). The HOMO and lowest-unoccupied molecular orbital (LUMO) energy levels of the donor polymers and NFAs were determined from the onset oxidation potential ($E_{\text{ox}}^{\text{onset}}$) and $E_g^{\text{opt}} - E_{\text{HOMO}}$, respectively, using the following electrochemical Equation (1)

$$E_{\text{HOMO}} = -4.8 - (E_{\text{ox}}^{\text{onset}} - E_{1/2,\text{ferrocene}}) \quad (1)$$

where $E_{1/2,\text{ferrocene}} = 0.49$ eV (measured data). As a result, the HOMO levels of the donor polymers decreased in the order of P(Cl), P(Cl)(F = 0.5), and P(F-Cl) to -5.47 , -5.56 , and -5.64 eV, respectively. These results, which are the effects of fluorine from an increased F-2DBDT level in the polymer backbones, match the results of the simulated DFT computation.^[23] NFAs showed deeper HOMO levels of -5.65 , -5.68 , and -5.71 eV for ITIC-Th, IDIC, and IT-4F, respectively. These trends were also found in the LUMO levels of NFAs. Therefore, the increase in the high open-circuit voltage (V_{oc}) in the order of IT-4F, IDIC, and ITIC-Th and the effective

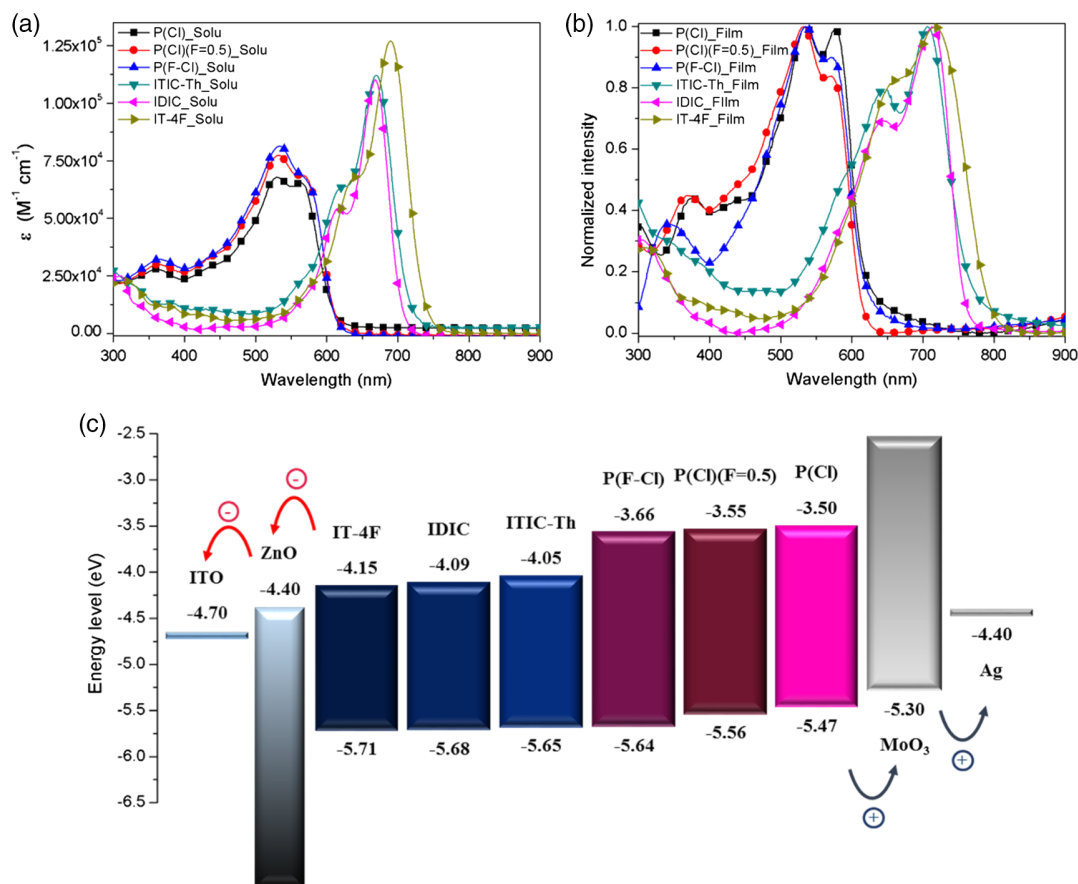


Figure 1. UV-vis absorption spectra and energy band diagrams from CV curves of donor polymers and NFAs: a) average molar absorption coefficients for 10^{-5} M chloroform solutions, b) UV-vis absorption spectra of chloroform solutions versus thin films, and c) energy band diagrams with inverted structures used in this study.

alignment of energy levels were expected when the donor polymers and NFAs were blended, as shown in Figure 1c.^[15] However, in some donor polymers and NFA combinations, because the energy offsets of the HOMO levels were within the narrow range of 0.01–0.04 eV, the probability of charge recombination was expected to be high.^[15,28–31] The details of the optical and electrochemical properties of donor polymers are shown in Table 2. The detailed values of NFAs are shown in Table S2, Supporting Information.

2.3. Photovoltaic Performance

To obtain the best performance based on P(Cl)(F = 0.5), all the devices were fabricated and optimized with each NFA (ITIC-Th, IDIC, and IT-4F) and compared with the previous results obtained for P(Cl) and P(F-Cl).^[14,15] Inverted device configurations of ITO/ZnO/donor polymer:NFA/MoO₃/Ag were fabricated to obtain better device stability than that in conventional devices using the high work-function metal anode.^[32] Detailed

Table 2. Optical and electrochemical properties of donor polymers.

| Polymer | UV-vis absorption | | | | CV | | | |
|----------------|-----------------------------|--|-----------------------------|--|------------------------------|---------------------------------------|--------------------------------------|---|
| | Chloroform solution | | Film | | $E_g^{\text{opt,a}}$ [eV] | $E_{\text{ox}}^{\text{onset}}$ [V] | $E_{\text{HOMO}}^{\text{b)}$ [eV] | $E_{\text{LUMO}}^{\text{b),c)}$ [eV] |
| | λ_{max} [nm] | Molar absorption coefficient ϵ [$\text{M}^{-1} \text{cm}^{-1}$] at λ_{max} [nm] | λ_{max} [nm] | | | | | |
| P(Cl) | 361, 530, 562 | 27 837 (361), 67 929 (530), 65 408 (562) | 376, 535, 578 | | 1.97 | 1.16 | −5.47 | −3.50 |
| P(Cl)(F = 0.5) | 363, 532, 562 | 29 897 (363), 77 374 (532), 67 929 (562) | 369, 533, 571 | | 2.01 | 1.25 | −5.56 | −3.55 |
| P(F-Cl) | 361, 533 | 32 172 (361), 81 299 (533) | 342, 535, 571 | | 1.99 | 1.34 | −5.64 | −3.66 |

^{a)} Calculated from the intersection of the tangent on the low energetic edge of the absorption spectrum with the baseline; ^{b)} $E_{\text{HOMO}} = -[E_{\text{ox}}^{\text{onset}} (\text{vs Ag/AgCl}) - E_{1/2}(\text{Fc/Fc}^+ \text{ vs Ag/AgCl})] - 4.8 \text{ eV}$; $E_{\text{LUMO}} = E_g^{\text{opt}} - E_{\text{HOMO}}$; ^{c)} $E_{1/2}(\text{Fc/Fc}^+ \text{ vs Ag/AgCl}) = 0.49 \text{ eV}$ (measured data).

information on the optimized devices is given in the Supporting Information. The current density–voltage (J - V) and external quantum efficiency (EQE) curves and their parameters for OSC performance are shown in Figure S7 and Table S3, Supporting Information. As a result, P(Cl)($F = 0.5$):IDIC exhibited the best performance with an efficiency of 12.1% due to the relatively high J_{sc} and fill factor (FF) values among the polymer blends (11.8% for P(F-Cl):IT-4F and 11.4% for P(Cl):ITIC-Th). This is because the compatibility between the donor and acceptor for P(Cl)($F = 0.5$):IDIC was the highest and the offset difference between the HOMO energy levels was optimal, increasing the charge carrier separation probability.^[28,29,31,33] The detailed studies analyzing the photoluminescence, morphology, and charge carrier mobility are shown in Supporting Information (Figure S8–S12 and Table S4 and S5, Supporting Information).

J - V and EQE curves of the optimized devices for P(Cl):ITIC-Th, P(Cl)($F = 0.5$):IDIC, and P(F-Cl):IT-4F are shown in Figure 2a,b, respectively, and the associated parameters are shown in Table 3. In particular, to conduct a reliability test for the P(Cl)($F = 0.5$):IDIC cell, which shows the highest PCE among the donor polymers, the device was encapsulated using an epoxy adhesive without any getter or UV protector. We requested measurements from the NCPAC, Republic of Korea (NO. 18S-0708), for certification. As shown in Figure 2c, a maximum certified PCE of 12.48% was recorded (Figure S13, Supporting Information). In addition, the continuous light and shelf life stability of optimized devices for P(Cl):ITIC-Th, P(Cl)($F = 0.5$):IDIC, and P(F-Cl):IT-4F were investigated with and without encapsulation (Figure S14, Supporting Information and Figure 2d). The photostability test was performed for over

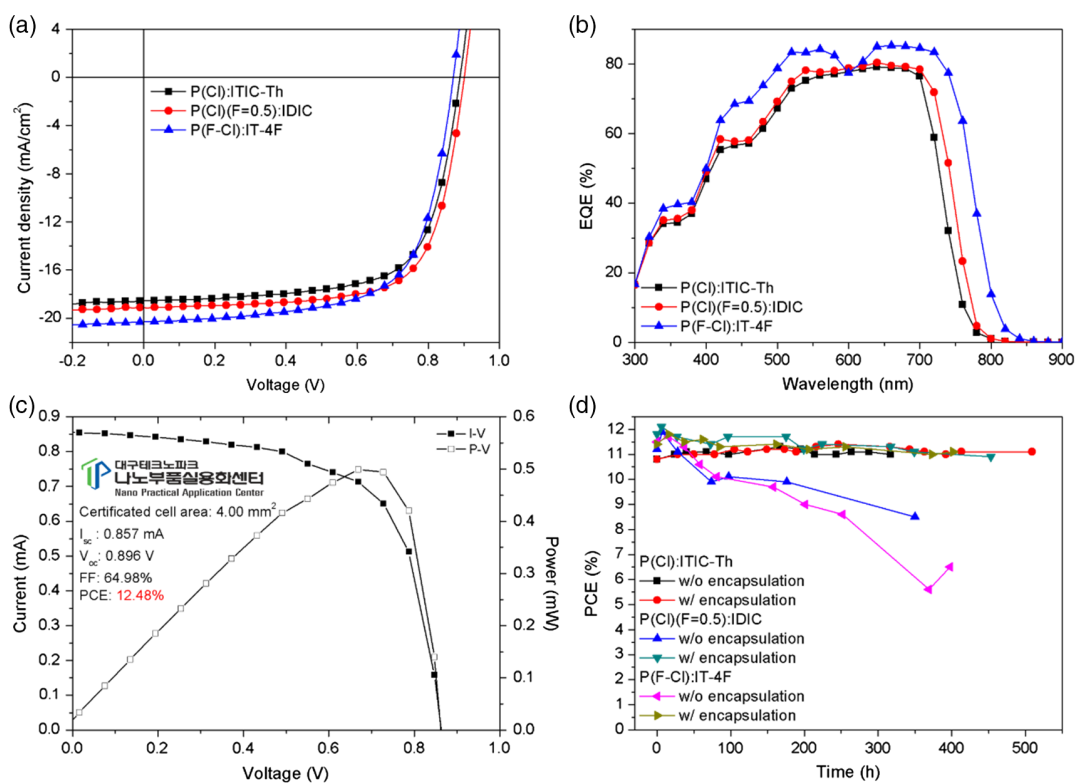


Figure 2. a) J - V , b) EQE curves, c) the photovoltaic results of the device with the greatest level of efficiency based on P(Cl)($F = 0.5$):IDIC, as certified by the NCPAC in the Republic of Korea (no. 18S-0708), d) long-lifetime stability results obtained using the ISOS-D-1 shelf protocol for optimized polymer blends for inverted OSCs.

Table 3. Photovoltaic performance of optimized polymer blends for inverted OSCs.

| Active layer | Thickness [nm] | Temperature ^{a)} [°C] | V_{oc} [V] | J_{sc} [mA cm^{-2}] | FF [%] | $\text{PCE}_{\text{max}}/\text{PCE}_{\text{ave}}^{\text{b)}}$ [%] |
|---|----------------|--------------------------------|--------------|----------------------------------|--------|---|
| P(Cl):ITIC-Th = 1:1.25 | 120 | 120 | 0.899 | 18.6 | 68.1 | 11.4/11.2 \pm 0.21 |
| P(Cl)($F = 0.5$):IDIC = 1:1 | 120 | 140 | 0.899 | 19.1 | 70.6 | 12.1/11.8 \pm 0.29 |
| P(Cl)($F = 0.5$):IDIC = 1:1 ^{c)} | | | 0.896 | 21.43 | 64.98 | 12.48 |
| P(F-Cl):IT-4F = 1:1 | 95 | 140 | 0.879 | 20.3 | 66.0 | 11.8/11.5 \pm 0.30 |

^{a)}Postannealing for 10 min; ^{b)}Average PCE values are calculated from ten independent cells; ^{c)}Certification result from the NCPAC, Republic of Korea (No. 18S-0708).

40 h in an air-conditioned environment at room temperature and 40% humidity under the continuous illumination of AM 1.5 G xenon lamp with 100 mW cm^{-2} . The performance of all devices slightly decreased, $\approx 10\%$ compared with each initial PCE due to burn-in loss. In spite of the fast light aging, P(Cl)(F = 0.5) and P(F-Cl) containing F-2DBDT showed the enhanced photostability during the whole time as compared with P(Cl) in conditions with and without encapsulation. Next, the shelf life stability test was studied by storing the devices in the same condition with the photostability test for over 300 h, and, subsequently, the ISOS-D-1 shelf protocol was implemented.^[13,14,34–36] As a gauge of device stability, the J - V characteristics of optimized devices with and without encapsulation were evaluated as a function of the storage time in terms of the corresponding photovoltaic parameters (Figure S15–S17, Supporting Information). The effect of aging on the photovoltaic parameters of OSCs during long-term storage, with and without encapsulation, is clearly demonstrated. P(Cl):ITIC-Th was already tested in a previous study.^[14] First, the initial devices for the PCEs of P(Cl)(F = 0.5):IDIC with and without encapsulation showed 11.8% and 11.2%, which gradually increased to 6 and 7 h, respectively, at which point the maximum PCEs were observed (without encapsulation: PCE = 11.9%, $V_{oc} = 0.899 \text{ V}$, $J_{sc} = 19.2 \text{ mA cm}^{-2}$, and FF = 68.6%, with encapsulation: PCE = 12.1%, $V_{oc} = 0.899 \text{ V}$, $J_{sc} = 19.1 \text{ mA cm}^{-2}$, and FF = 70.1%). Next, although the initial devices for P(F-Cl):IT-4F, with and without encapsulation, showed PCEs of 11.4% and 11.5%, the efficiencies gradually increased when both devices exhibited the maximum PCEs after 16 h (without encapsulation: PCE = 11.7%, $V_{oc} = 0.859 \text{ V}$, $J_{sc} = 21.3 \text{ mA cm}^{-2}$, and FF = 64.0%, with encapsulation: PCE = 11.8%, $V_{oc} = 0.879 \text{ V}$, $J_{sc} = 20.3 \text{ mA cm}^{-2}$, and FF = 66.0%). The cause of this increase is believed to be because of the relaxation of tilt generated by the presence of large Cl atoms in the polymer backbones; thus, the intermolecular/intramolecular packing order of each device is closer in proximity than that of their initial states.^[14] However, the blend of two polymers without encapsulation showed a significantly more drastic reduction in efficiency during the shelf lifetime stability measurements compared with the devices with encapsulation. For P(Cl)(F = 0.5):IDIC, the initial efficiency was 11.2%, which was reduced by 24.1% after 350 h (i.e., PCE = 8.5%). For P(F-Cl):IT-4F, the initial efficiency was 11.5%, which was reduced by 43.8% after 398 h (i.e., PCE = 6.5%).

As shown in Figure 3, this drastic change is attributable to the vulnerability of both combinations of polymers, P(Cl)(F = 0.5):IDIC and P(F-Cl):IT-4F, to moisture or oxygen. In other words, a phase separation in the morphology due to moisture or oxygen can result in low atmospheric stability with decrement of FF from too much aggregation or mixing that occurs reversibly over time.^[37–39] On the contrary, P(Cl):ITIC-Th showed excellent atmospheric stability without encapsulation, with an efficiency of 11.0%, which increased by 2% after 317 h compared with the initial efficiency of 10.8%. In addition, its efficiency only decreased by 9% despite measuring the long-term stability in atmosphere after 2002 h.^[14] The detailed parameters of photovoltaic performances for P(Cl)(F = 0.5):IDIC, P(F-Cl):IT-4F, and P(Cl):ITIC-Th with respect to encapsulation are shown in Table S6–S8, Supporting Information.

To help a more detailed understanding of the shelf life stability difference of each polymer blend, fresh active layers were spin coated on top of the ITO/ZnO substrate as each optimized conditions. The films were stored in the same environment with a shelf life stability test and analyzed by atomic force microscopy (AFM) depending on time (pristine, 50, 200, and 350 h). As shown in Figure 4 and Figure S18, Supporting Information, all pristine blend films for P(Cl):ITIC-Th, P(Cl)(F = 0.5):IDIC, and P(F-Cl):IT-4F are fine and uniform with root-mean-square (RMS) roughness values of 1.26, 0.90, and 0.97 nm, respectively. During the test, P(Cl):ITIC-Th film maintains the same smooth and interpenetrating networks with similar RMS values in the range of 1.17–1.26 nm, except for the 50 h case. Though the partial aggregates of the film were observed to increase slightly after 300 h, there was no effect on the device performance. However, P(Cl)(F = 0.5):IDIC and P(F-Cl):IT-4F films showed a peculiar morphology behavior depending on time in comparison with P(Cl):ITIC-Th. In short, both films were observed and the aggregates were seen to gradually increase in size over time which may cause charge carrier recombination and low FF. The P(Cl)(F = 0.5):IDIC films showed many big islands with bright and dark regions in contrast and even the RMS values increased from 0.90 to 1.60 nm over time. In contrast, the P(F-Cl):IT-4F morphology showed that the nanofibril domains gradually disappear and also the RMS values decreased from 0.97 to 0.43 nm which may be inefficient in limiting the charge separation and transport in the vertical phase. This result means that the aggregation behaviors for P(Cl)(F = 0.5):IDIC and P(F-Cl):IT-4F differ from P(Cl):ITIC-Th. In addition, we investigated the thermal stability of the optimized polymer blends for 24 h at different temperatures (80 and 150 °C) to know whether they provide the same conclusion with stability tests. As shown in Figure S19–S21, Supporting Information, the tolerance of morphology for P(Cl):ITIC-Th, P(Cl)(F = 0.5):IDIC, and P(F-Cl):IT-4F was in turn ranked. Likewise, the changes of the RMS values largely increased according to annealing temperature and time which means that each material consisting of a morphology is more sensitive about thermal stress. Finally, we tested the shelf life stability of the devices without encapsulation of the optimized polymer blends processed by air atmosphere (at room temperature and 40% humidity for 300 h). More details of the photovoltaic parameters as a function of time for devices are shown in Figure S22, Supporting Information. To sum up, efficiencies of the optimized polymer blends decrease with ≈ 10 –20% due to the slight decrease in FF values in comparison with each device processed by the glove box. Although the morphology changes, as shown in Figure S23, Supporting Information, the shelf life stability trends are consistent with that in the previous study. Comprehensively, it directly is related to the inherent properties of components in each morphology. Therefore, the relationship between the crystallinity and miscibility of donor polymers and NFAs should be systematically investigated.

2.4. Crystal Packing Analysis

As demonstrated in Figure 5 2D, GIWAXS is an efficient approach toward investigating the crystallinity and molecular

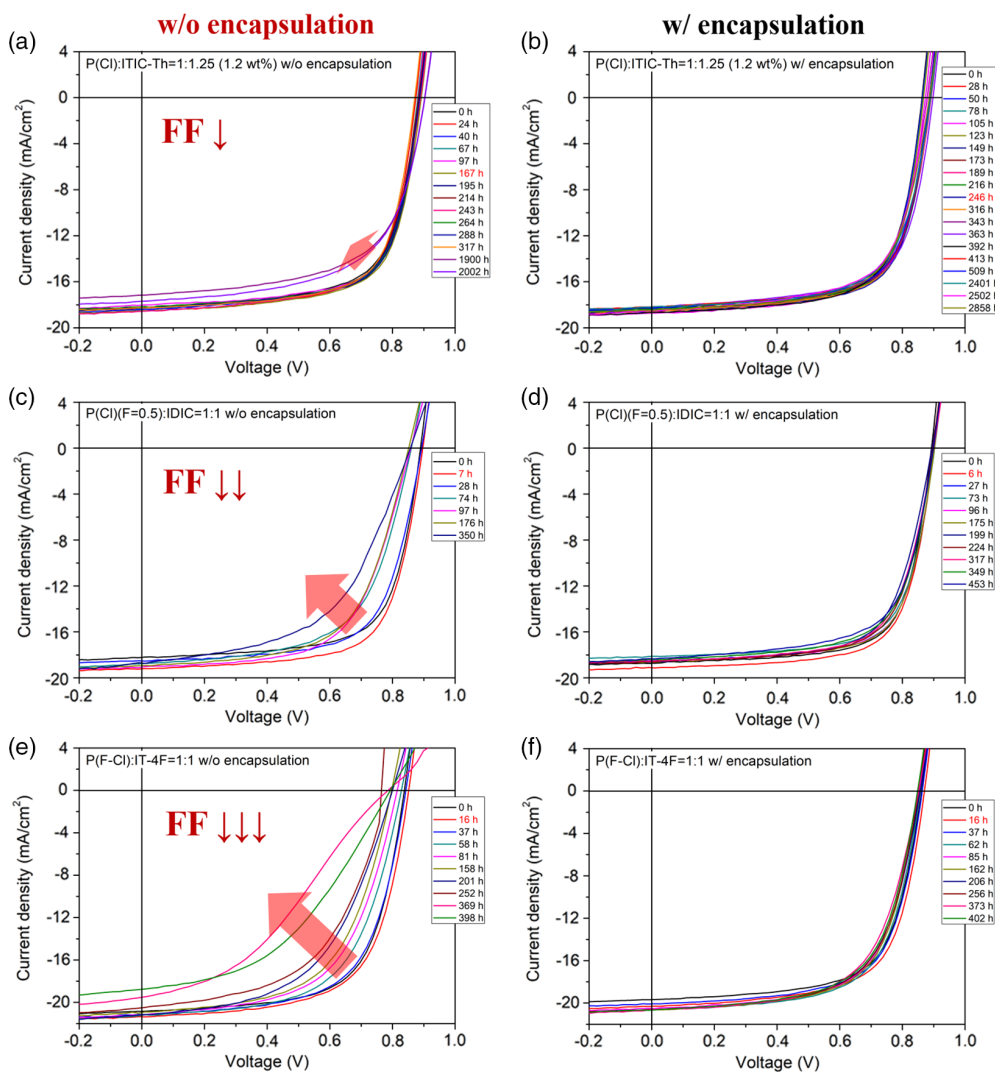


Figure 3. J - V curves of long lifetime stability tests obtained using the ISOS-D-1 shelf protocol for P(Cl):ITIC-Th = 1:1.25, P(Cl)(F = 0.5):IDIC = 1:1, and P(F-Cl):IT-4F = 1:1 a-c) without and d-f) with encapsulation for inverted OSCs.

orientation of the pristine donor polymers and NFA films.^[14] The 2D GIWAXS patterns (Figure 5a,b) and the corresponding out-of-plane (OOP) (along q_{xy}) and in-plane (IP, along q_z) profiles (Figure S24a-d, Supporting Information) of all the films, including donor polymers of P(Cl), P(Cl)(F = 0.5), and P(F-Cl) and NFAs of ITIC-Th, IDIC, and IT-4F, were obtained, respectively. In addition, an intensity-integrated azimuthal pole figure plot was constructed for the (100) scattering peaks of the pristine and blended polymer films (Figure S24e and S17f, Supporting Information). The integrated areas within the azimuthal angle (χ) in the ranges of 0–45° (A_z) and 45–90° (A_{xy}) are defined as the corresponding fractions of face-on and edge-on structures, respectively, and the ratio, A_{xy}/A_z , was calculated as a metric for the face-on-to-edge-on structure ratio. First, the donor polymers showed similar orientations on a ZnO substrate in bimodal form, with distinct (100) and (010) peaks in the OOP profiles. For all polymers, amorphous rings appeared around 1.4 \AA^{-1} due to the regiorandomness of the polymer backbones which was

increased by the introduction of asymmetric chlorinated thiophene.^[14] The amorphous ring was more pronounced in P(Cl)(F = 0.5) due to the increase in regiorandom segments as the polymer chains grew in the terpolymer form.^[40] Next, as shown in Figure S24a,c, Supporting Information, the comparison of plot data in OOP shows that the lamellar packing distance ($d(100)$) gradually reduced as the mole ratio of F-2DBDT units in the polymer backbones increased (100). In the case of (010) π - π stacking distances ($d(010)$), the P(Cl)(F = 0.5) polymers to which F-2DBDT was introduced at a mole ratio of 0.5 showed the closest packing properties. In addition, as shown in Figure 5c, using the full width at half maximum (FWHM) value calculated by extracting the plot data of donor polymers in OOP, crystal coherence lengths (CCLs (100) and CCL (010)) in (100) and (010) were calculated. CCL (100) values were found to increase in the order of P(F-Cl), P(Cl), and P(Cl)(F = 0.5), whereas CCL (010) values were found to increase in the order of P(F-Cl), P(Cl)(F = 0.5), and P(Cl). This indicates that the size of the crystal of (100) is

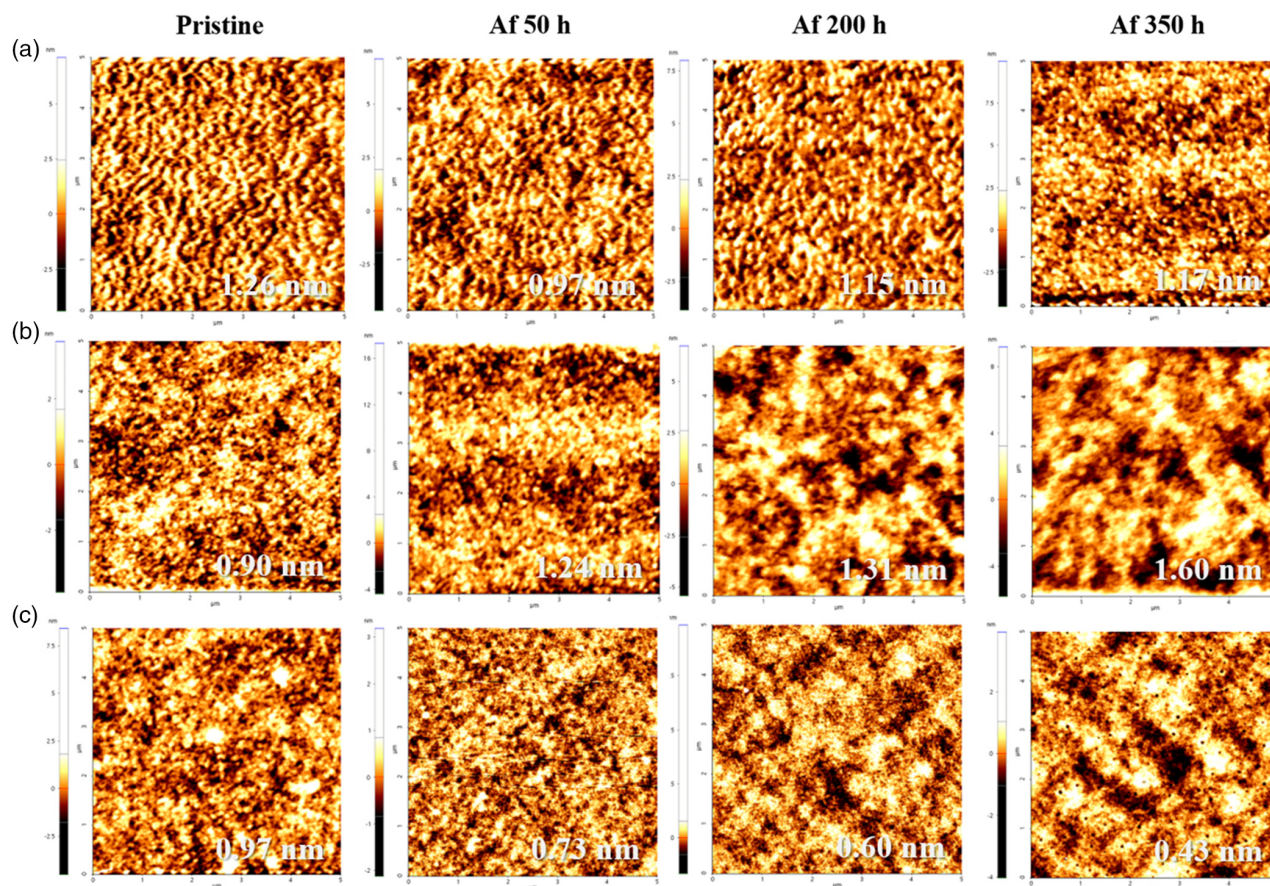


Figure 4. AFM 2D topography of optimized polymer blends over time (pristine, 50, 200, and 350 h). All images are 5–5 μm : a) P(Cl):ITIC-Th, b) P(Cl)(F = 0.5):IDIC, and c) P(F-Cl):IT-4F.

the largest in P(Cl)(F = 0.5) and that of (010) is the largest in P(Cl). Finally, the relative ratio (A_{xy}/A_z) of the face-on structure versus edge-on structure was obtained, as shown in Figure S24e, Supporting Information. The ratio was found to decrease in the order of P(Cl), P(F-Cl), and P(Cl)(F = 0.5), thus decreasing the face-on structure gradually. On the other hand, NFAs showed different crystallinities and orientations, as shown in Figure S24b,d, Supporting Information. A comparison and analysis of the plot data in OOP showed that the crystallinities and orientations got closer in the order of IDIC, IT-4F, and ITIC-Th for d (100) and in the order of IT-4F, IDIC, and ITIC-Th for d (010). Especially, IDIC showed a high crystallinity with long-range regularity for (200) and (300), as well as (100) in OOP. Furthermore, as shown in Figure 5c, the CCL (100) and CCL (010) of NFAs were calculated, which revealed that the size of the crystal shrunk in the order of IDIC, IT-4F, and ITIC-Th for (100) and in the order of IDIC, ITIC-Th, and IT-4F for (010), respectively. Finally, the A_{xy}/A_z ratios of NFAs were calculated, as shown in Figure S24f, Supporting Information. The ratios revealed that the face-on structure increases in the order of ITIC-Th, IT-4F, and IDIC. Therefore, considering these ratios in terms of crystallinity and orientation, when the donor polymers and NFAs are blended, the complementary face-on and edge-on ratios between the donor and acceptor can have balanced

crystallinities, showing excellent performance in combinations such as P(Cl):ITIC-Th, P(Cl)(F = 0.5):IDIC, and P(F-Cl):IT-4F.^[41–44] The values from the GIWAXS analysis and the calculated values are shown in Table 4 and Figure S9, Supporting Information.

2.5. Miscibility Analysis

To thoroughly compare the miscibility of donor polymers and NFAs, the surface tension (γ) between the polymer donor and acceptor was investigated.^[17,22] The γ values can be calculated from the contact angles of two solvents (water and oil) on neat films, as in the Wu model.^[17,18,21,22] In Figure S25, Supporting Information, the contact angles of water and oil (diiodomethane, DIM) in the pristine material films exhibit different trends. As a result, the surface tension values of the donor polymers gradually decrease as the mole ratio of the F-2DBDT unit increases. This means that both noncovalent interactions within and outside the molecular structure increase with the introduction of F, resulting in lower surface energy values.^[45–47] In the case of NFAs, surface tension values decreased in the order of ITIC-Th, IT-4F, and IDIC.^[20,22] Particularly, in regard to IDIC, as aliphatic chains are introduced into an indacenodithiophene (IDT) core instead of aromatic alkyl chains, IDIC had the lowest surface energy due

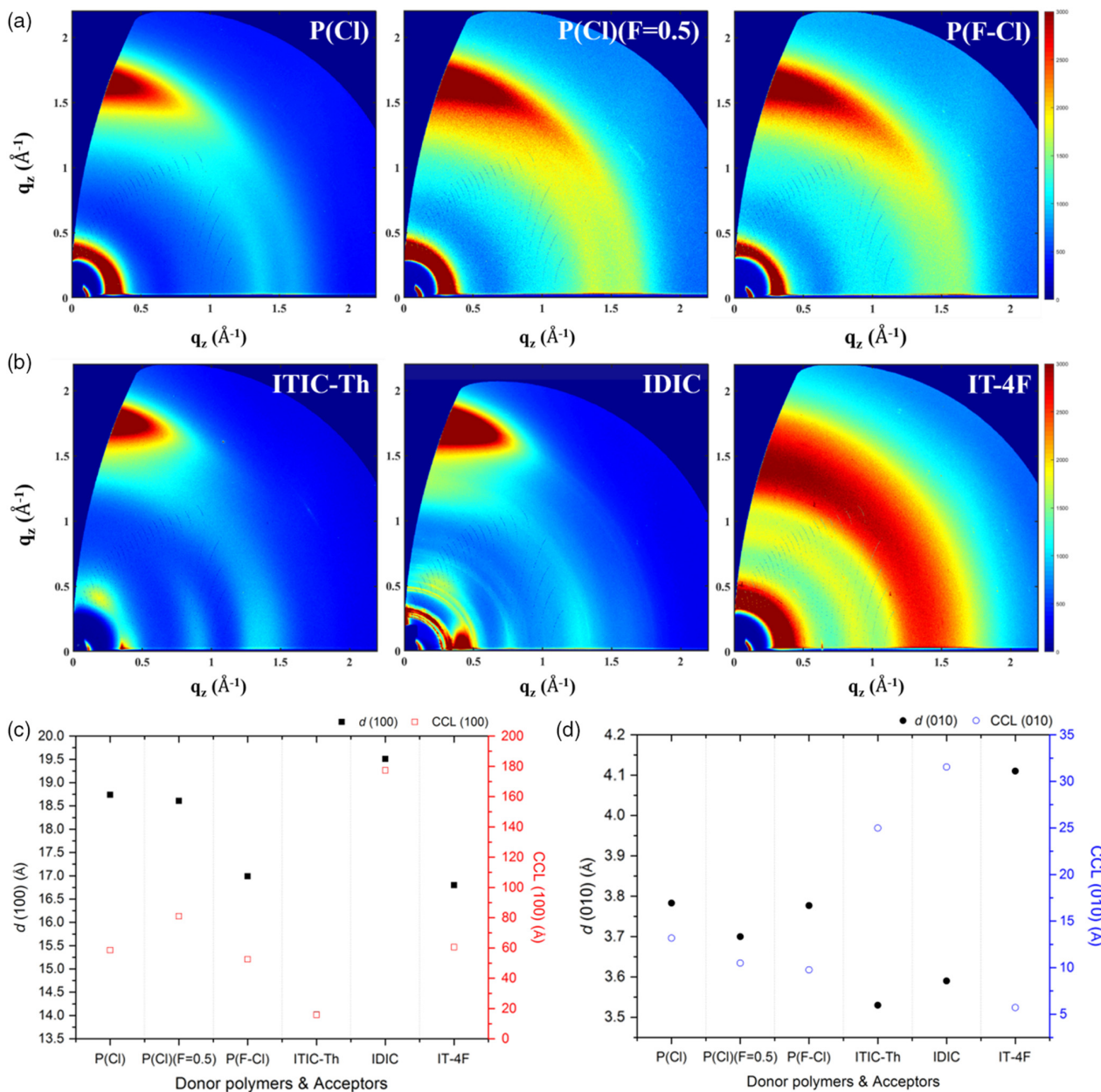


Figure 5. 2D GIWAXS data for pristine materials. The 2D GIWAXS patterns of a) donor polymers: P(Cl), P(Cl)(F = 0.5), and P(F-Cl) and b) NFAs: ITIC-Th, IDIC, and IT-4F; c) lamellar packing distances ($d(100)$) versus its CCLs (CCL(100)) and d) π - π stacking distances ($d(010)$) versus its CCLs (CCL(010)) estimated from the (100) lamellar and (010) π - π stacking diffraction, respectively, in the OOP profiles.

to the higher π - π stacking interactions between molecular structures compared with ITIC-Th and IT-4F.^[19,22,48] On the contrary, the energy barrier of IT-4F was lower than that of ITIC-Th because of the two F atoms that were introduced at each end. As a result, stronger noncovalent interactions were possible in molecular packing.^[49] The blend miscibility was estimated by applying these data and the corresponding γ values in the Flory-Huggins interaction parameter (χ), which is based on the surface tension data, using Equation (2).^[17,18,21,22]

$$\chi = (\sqrt{\gamma_D} - \sqrt{\gamma_A})^2 \quad (2)$$

In general, as the χ values decrease, the miscibility between the two components increases, and as a result, the domain purity decreases to cause poor morphology and lower efficiency. On the other hand, if the χ values are too large, the miscibility between the two components decreases excessively that it will result into a too pure phase, leading to an increase in charge recombination and a decrease in efficiency.^[7,16–22] Therefore, finding a donor-acceptor combination that has the appropriate degree of miscibility is essential to obtaining efficient OSCs.^[17,18,21,22,47–49] Detailed values are shown in **Table 5**. However, the results cannot be directly correlated with the photovoltaic performance

Table 4. GIWAXS results for pristine donor polymers and NFAs in OOP.

| | d (100) ^{a)} [Å] at (100) [Å ⁻¹] | d (200) ^{a)} [Å] at (200) [Å ⁻¹] | d (300) ^{a)} [Å] at (300) [Å ⁻¹] | d (010) ^{a)} [Å] at (010) [Å ⁻¹] | A_{xy}/A_z ^{b)} |
|--------------------|--|--|--|--|----------------------------|
| P(Cl) | 18.74 at 0.335 | – | – | 3.78 at 1.663 | 1.29 |
| P(Cl)($F = 0.5$) | 18.61 at 0.337 | – | – | 3.70 at 1.700 | 0.95 |
| P(F-Cl) | 16.99 at 0.370 | – | – | 3.78 at 1.662 | 1.21 |
| ITIC-Th | 14.02 at 0.448 | – | – | 3.53 at 1.779 | 1.04 |
| IDIC | 19.51 at 0.322 | 13.32 at 0.472 | 6.37 at 0.986 | 3.59 at 1.750 | 1.27 |
| IT-4F | 16.80 at 0.374 | – | – | 4.11 at 1.530 | 1.05 |

^{a)} q_{xy} (or q_z) = $2\pi/d$ (010) (or d ($h00$)); ^{b)}The ratio of face-on-to-edge-on orientation determined by the pole figure analysis, where A_{xy} and A_z correspond to the face-on and edge-on fractions.

Table 5. Contact angles of water and DIM, and their values for pristine donor polymers and NFAs.

| Surface | θ_{water} [°] | θ_{DIM} [°] | γ [mN m ⁻¹] | χ |
|--------------------|-----------------------------|---------------------------|--------------------------------|---|
| P(Cl) | 93.7 | 47.4 | 35.72 | 0.757 ^{a)} /0.121 ^{b)} /0.303 ^{c)} |
| P(Cl)($F = 0.5$) | 95.0 | 49.1 | 34.78 | 0.901 ^{a)} /0.182 ^{b)} /0.397 ^{c)} |
| P(F-Cl) | 95.2 | 51.5 | 33.44 | 1.132 ^{a)} /0.293 ^{b)} /0.555 ^{c)} |
| ITIC-Th | 92.3 | 23.7 | 46.88 | – |
| IDIC | 104.1 | 41.8 | 39.99 | – |
| IT-4F | 93.9 | 34.1 | 42.61 | – |

^{a)}The Flory–Huggins interaction (χ) values of polymer ITIC-Th; ^{b)}The Flory–Huggins interaction (χ) values of polymer IDIC; ^{c)}The Flory–Huggins interaction (χ) values of polymer IT-4F.

which means that the miscibility should be analyzed in each blend system with the crystallinity analysis.

2.6. Correlation between Molecular Ordering and Miscibility

The crystallinity and miscibility for NFAs and polymer blends were further investigated by carrying out DSC measurements (Figure S26, Supporting Information).^[50–55] Three polymers already exhibited an amorphous nature with ductility, as explained in the previous section. The pure NFAs of ITIC-Th, IDIC, and IT-4F exhibit exothermic crystalline temperatures (T_c) with crystallizing tendencies at 234.17, 177.29, and 214.08 °C, respectively, whereas only ITIC-Th and IDIC possess endothermic melting temperatures (T_m) with melting enthalpies (ΔH_m) at 298.85 °C (67.64 J g⁻¹) and 284.55 °C (93.18 J g⁻¹). As shown in Figure S26a, Supporting Information, all polymer blends with IT-4F showed no detectable thermal transition, indicating that IT-4F-based polymer blends have a relative high miscibility between both components.^[53–55] After blending with IDIC, the melting temperatures of all polymers showed a slight change ranging from 0.45 to 1.69 °C, whereas their melting enthalpies were approximately reduced by half. Based on the comparison of ΔH_m (Figure S26b, Supporting Information), molecular packing is in the order of P(Cl) (45.46 J g⁻¹), P(Cl)($F = 0.5$) (48.06 J g⁻¹), and P(F-Cl) (59.23 J g⁻¹). In other

words, all polymer blends with IDIC maintain a high crystalline nature and pure domains of IDIC due to low miscibility.^[51] Finally, in the case of ITIC-Th, all polymer blends possess first and right after second melting temperatures (T_m^1 and T_m^2) each with different melting enthalpies (ΔH_m^1 and ΔH_m^2). As shown in Figure S26c, Supporting Information, the T_m^1 is an obvious transition peak of the inherent ITIC-Th nature; the ΔH_m^1 decreases by two-thirds in pure ITIC-Th. This means that polymer blends with ITIC-Th showed a relatively lower crystallinity compared with IDIC-based polymer blends.^[52] T_m^2 is estimated to result from phase transitions due to the observation made at 277.19–279.71 °C. In addition, the values of ΔH_m^2 of P(F-Cl) (1.773 J g⁻¹), P(Cl) (5.932 J g⁻¹), and P(Cl)($F = 0.5$) (9.398 J g⁻¹) suggest that all polymers possess crystal-like behavior when blended, which is consistent with the GIWAXS results from the tendency of the CCL (100) for P(F-Cl) (52.478 Å), P(Cl) (58.496 Å), and P(Cl)($F = 0.5$) (80.961 Å). As a result, P(Cl):ITIC-Th is well ordered according to the values of ΔH_m^1 and ΔH_m^2 between both pure domains. The crystallinity exhibited by P(Cl)($F = 0.5$):IDIC or P(F-Cl):IDIC was too high, whether in the polymer or in IDIC. In summary, the miscibility of the polymer blends increased in the order of IDIC, ITIC-Th, and IT-4F based on the molecular interaction between the donor and acceptor in each blend.

To thoroughly investigate the difference in atmospheric stability among the three polymer blends, as shown in Figure 6, 2D GIWAXS was used to analyze the crystallinity and orientation of optimized polymer blend films. The 2D GIWAXS patterns (Figure 6a) and the corresponding OOP and IP profiles (Figure S27a,b, Supporting Information) of the three films, P(Cl):ITIC-Th, P(Cl)($F = 0.5$):IDIC, and P(F-Cl):IT-4F, were obtained. In addition, intensity-integrated azimuthal pole figure plots for the (100) scattering peaks of the pristine and blended polymer films were constructed (Figure S27c, Supporting Information). A complementary enhancement in the packing order properties on ZnO substrates was observed in the optimized polymer blends compared with each pristine state.^[7,16–22,47–49] The three polymer blends exhibited an amorphous ring at ≈ 1.4 Å⁻¹. The ring was the most intense in P(F-Cl):IT-4F, followed by P(Cl):ITIC-Th and P(Cl)($F = 0.5$):IDIC. Upon the detailed investigation of the polymer blend films, P(Cl):ITIC-Th exhibited four distinct peaks, with balanced crystallinity between the donor and acceptor, thus exhibiting the closest π – π stacking distance along

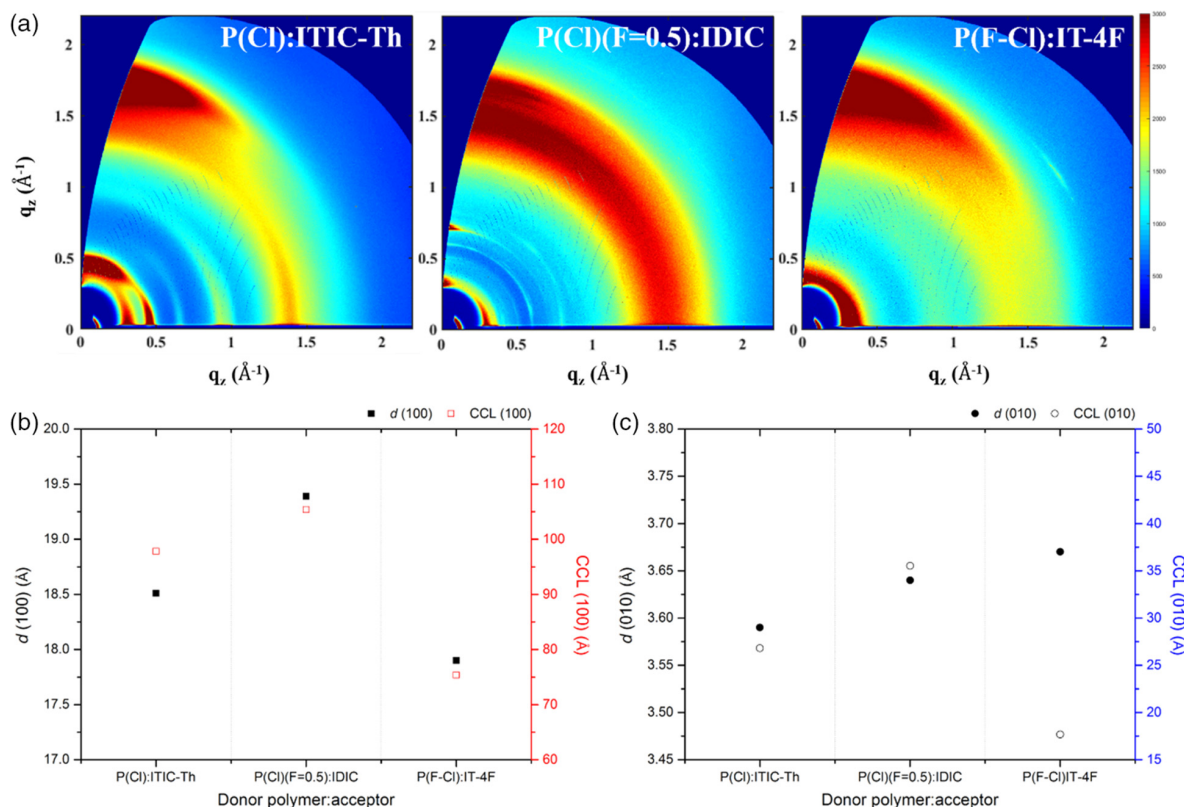


Figure 6. 2D GIWAXS data for optimized polymer blends. a) The 2D GIWAXS patterns of P(Cl):ITIC-Th, P(Cl)(F = 0.5):IDIC, and P(F-Cl):IT-4F; b) lamellar packing distances ($d(100)$) versus its CCLs (CCL(100)); and c) π - π stacking distances ($d(010)$) versus its CCLs (CCL(010)) estimated from the (100) lamellar and (010) π - π stacking diffraction, respectively, in the OOP profiles.

with the strong face-on structures. However, the A_{xy}/A_z ratio of P(Cl):ITIC-Th was 0.82, which confirmed that the edge-on structure was relatively more dominant. In P(Cl)(F = 0.5):IDIC, as the IDIC—which had the highest crystallinity and the strongest face-on structure among the NFAs—was introduced, the polymers (100) and (200) and NFAs (100) were strongly exhibited. In addition, the low A_{xy}/A_z ratio in the pristine polymer increased to 1.15 after blending, confirming that the face-on structure was relatively more dominant. Finally, the most compact (100) lamellar packing order in the polymer blends was observed in P(F-Cl):IT-4F, where the A_{xy}/A_z ratio was 1.46. This ratio implied that P(F-Cl):IT-4F had the greatest face-on-structure-dominant orientation. Detailed parameters from the plot data of the blended films are shown in Table 6.

Next, the lamellar packing distance ($d(100)$) versus the (100) CCLs (100) and π - π stacking distance ($d(010)$) versus the CCLs (010) were determined using the OOP (010) peaks (Figure 6b,c), respectively. The parameters are shown in Table S10, Supporting Information. According to the results, P(Cl):IDIC blend exhibited the largest (100) and (010) crystals, followed by P(Cl):ITIC-Th and P(F-Cl):IT-4F. For further analysis, CCL(010) versus CCL(100), or CCL(010)/CCL(100), in OOP was calculated and compared, and the CCL(010)/CCL(100) values of P(Cl)(F = 0.5):IDIC, P(Cl):ITIC-Th, and P(F-Cl):IT-4F were 0.337, 0.274, and 0.234, respectively. From a crystallographic point of view, these results imply that the three polymer blends adhere to these tendencies when the size of the crystal is bound to increase or decrease with time reversibly. In other words,

Table 6. GIWAXS results for optimized polymer blends in the OOP direction.

| | $d(100)^a$ [Å] at (100) [Å ⁻¹] | $d(100)_{\text{NFA}}^a$ [Å] at (100) [Å ⁻¹] | $d(200)^a$ [Å] at (200) [Å ⁻¹] | $d(200)_{\text{NFA}}^a$ [Å] at (200) [Å ⁻¹] | $d(010)^a$ [Å] at (010) [Å ⁻¹] | A_{xy}/A_z^b |
|---------------------|--|---|--|---|--|----------------|
| P(Cl):ITIC-Th | 18.51 at 0.339 | 13.32 at 0.472 | – | 6.37 at 0.986 | 3.59 at 1.750 | 0.82 |
| P(Cl)(F = 0.5):IDIC | 19.39 at 0.324 | 12.22 at 0.514 | 8.79 at 0.715 | – | 3.64 at 1.726 | 1.15 |
| P(F-Cl):IT-4F | 17.90 at 0.351 | – | – | – | 3.67 at 1.711 | 1.46 |

^{a)} q_{xy} (or q_z) = $2\pi/d(010)$ (or $d(h00)$); ^{b)} The ratio of face-on-to-edge-on orientation determined by the pole figure analysis, where A_{xy} and A_z correspond to the face-on and edge-on fractions.

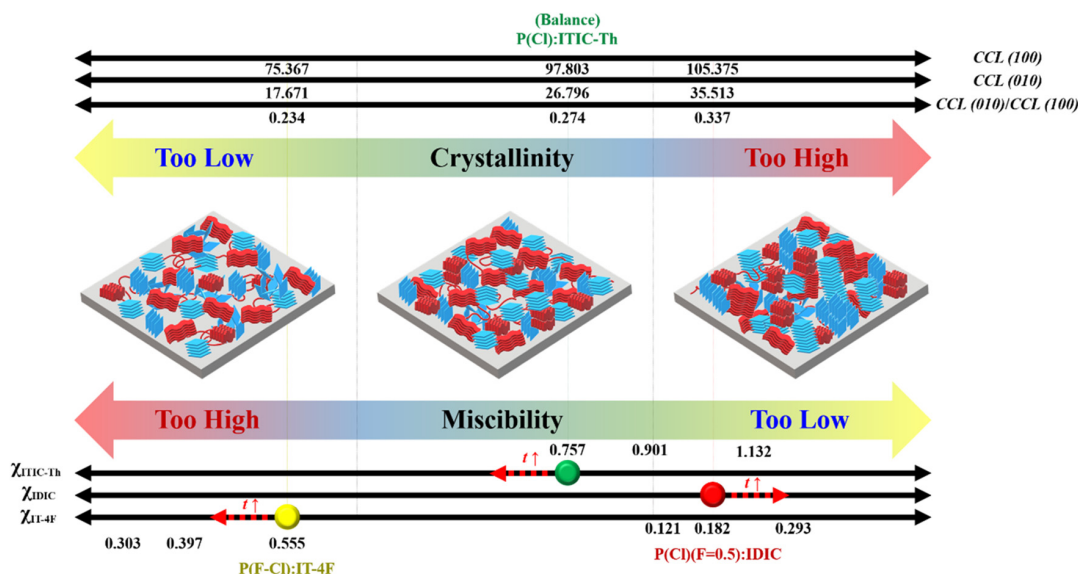


Figure 7. Schematic of the influence of correlation between crystallinity and miscibility for optimized polymer blends: red and blue objects in the boxes represent the donor polymers and NFAs, respectively.

optimized polymer blends change over time in the atmosphere due to thermodynamically reversible reactions in the crystals, which then causes the sizes of the crystals to increase or decrease, causing too much aggregation or mixing, which leads to phase separation. This in turn leads to a reduction in efficiency with respect to the long-term stability of the device.^[37–39]

Comprehensively, the chart can be summarized and listed in relation to optimized photovoltaic performances in terms of key factors for crystallinity and miscibility (**Figure 7**). First, the level of efficiency of P(Cl)(F = 0.5):IDIC was the highest at 12.1% due to the initially balanced A_{xy}/A_z ratios of 1.15. However, due to the relatively high CCL (010)/CCL (100) of 0.337 and very low miscibility level, the aggregation of each component or between two components gradually increased over time, leading to the formation of an extremely pure phase and decreasing the level of efficiency to 8.5% after 350 h.^[37–39,56] Second, the A_{xy}/A_z ratio in P(F-Cl):IT-4F was 1.46, which implied a dominant face-on structure. Initially, P(F-Cl):IT-4F showed a high efficiency of 11.8%. However, due to the relatively low CCL (010)/CCL (100) of 0.234 and very high miscibility level, the degree of mixing between the two components increased over time and formed an extremely miscible phase after 398 h. This resulted in a poor efficiency level of 6.5%.^[37–39,56] Finally, the initial A_{xy}/A_z ratio for P(Cl):ITIC-Th was 0.82, which indicated a dominant edge-on structure, and a relatively moderate (100) and (010) crystal size (CCL (010)/CCL (100): 0.274), balancing its crystallinity and miscibility. Therefore, its initial efficiency of 10.8% was increased to a maximum efficiency of 11.4% after 246 h and was maintained at 11.0% after 317 h, thus exhibiting the highest atmospheric stability among polymer blends.^[14] After conducting this case study, it was concluded that the correlation between crystallinity and miscibility of donor polymers and NFAs has a significant effect on the efficiency and stability of the device.^[57]

3. Conclusion

A new chlorinated thiophene-based donor terpolymer, P(Cl) (F = 0.5), was successfully designed and synthesized by modifying the previously reported P(Cl) and P(F-Cl), to better match their energy levels and compatibility with that of NFAs. As a result, the combination of P(Cl)(F = 0.5) with IDIC attained the highest PCE (12.1%) among the optimized polymer blends. In addition, the correlation between the crystallinity and miscibility of neat (P(Cl), P(Cl)(F = 0.5), P(F-Cl), ITIC-Th, IDIC, and IT-4F) and blend materials (P(Cl):ITIC-Th, P(Cl)(F = 0.5), and P(F-Cl):IT-4F) was closely investigated to understand all the different shelf life stability behaviors. A deep correlation between crystallinity (CCL) and miscibility (Flory–Huggins interaction) of donor polymers and NFAs was found to be related to the air stability of optimized NFOSC. This finding suggests that an optimal balance between moderate crystallinity and miscibility is essential for the achievement of high-air stable NFOSCs. This study will provide valuable guidelines for optimizing systems of donor polymers and NFAs to obtain highly efficient and stable OSCs.

4. Experimental Section

Polymerization: Scheme 1 outlines the synthetic routes for the polymer. The characterization results of the polymer are illustrated in the Supporting Information (Figure S1, Supporting Information).

Poly[(2,6-(4,8-bis(5-(2-ethylhexyl)thiophen-2-yl)-benzo[1,2-b:4,5-b'] dithiophene))-(2,6-(4,8-bis(5-(2-ethylhexyl)-4-fluorothiophen-2-yl)-benzo[1,2-b:4,5-b'] dithiophene))-alt-(2,5-(3-chlorothiophene))] (P(Cl)(F = 0.5)): a mixture of M2 (90.45 mg, 0.10 mmol), M3 (94.05 mg, 0.10 mmol), M1 (55.3 mg, 0.20 mmol), and Pd(pph₃)₄ (8.0 mg) was placed in a 10–20 mL vial in air. The vial was capped and vacuumed for 20 min before it was refilled with nitrogen gas, after which anhydrous toluene (6.0 mL) was added to the mixture. The reactor was degassed twice and refilled with nitrogen.

The polymerization mixture was stirred at 100 °C for 3 h. The polymer was end capped by the addition of 2-bromothiophenes (56.0 mg, 0.33 mmol), and the mixture was further heated at 140 °C for 1 h. After heating, 2-tributylstannyl thiophene (31.3 mg, 0.0875 mmol) was added and the mixture was heated once more at 140 °C for 1 h. The reaction mixture was cooled to room temperature and poured into methanol (300 mL) and 37% HCl (10 mL), after which it was stirred for 1 h, and then purified further through a Soxhlet extractor with methanol, acetone, hexane, methylene chloride, ethyl acetate, and chloroform, sequentially. The chloroform fraction of the polymer was reprecipitated in methanol, filtered, and vacuum dried. P(CI)(F = 0.5), dark red solid, yield: 85%.

Supporting Information

Supporting Information is available from the Wiley Online Library or from the author.

Acknowledgements

This research was supported by the New & Renewable Energy Core Technology Programs (nos. 20153010140030 and 20193091010110) and the Human Resources Program (no. 20194010201790) of the Korea Institute of Energy Technology Evaluation and Planning (KETEP) grant, funded by the Ministry of Trade, Industry & Energy, Republic of Korea.

Conflict of Interest

The authors declare no conflict of interest.

Keywords

chlorinated thiophene, donor polymers, nonfullerene organic solar cells

Received: February 7, 2020

Revised: April 15, 2020

Published online: May 13, 2020

- [1] S. R. Forrest, *Nature* **2004**, *428*, 911.
- [2] T. Kim, J.-H. Kim, T. E. Kang, C. Lee, H. Kang, M. Shin, C. Wang, B. Ma, U. Jeong, T.-S. Kim, B. J. Kim, *Nat. Commun.* **2015**, *6*, 8547.
- [3] J. Yuan, Y. Zhang, L. Zhou, G. Zhang, H.-L. Yip, T.-K. Lau, X. L. C. Zhu, H. Peng, P. A. Johnson, M. Leclerc, Y. Cao, J. Ulanski, Y. Li, Y. Zou, *Joule* **2019**, *3*, 1140.
- [4] B. Fan, D. Zhang, M. Li, W. Zhong, Z. Zeng, L. Ying, F. Huang, Y. Cao, *Sci. China Chem.* **2019**, *62*, 746.
- [5] Q. An, X. Ma, J. Gao, F. Zhang, *Sci. Bull.* **2019**, *64*, 504.
- [6] Y. Wang, X. Ke, Z. Xiao, L. Ding, R. Xia, H. Yip, *Science* **2018**, *361*, 1094.
- [7] G. Zhang, J. Zhao, P. C. Y. Chow, K. Jiang, J. Zhang, Z. Zhu, J. Zhang, F. Huang, H. Yan, *Chem. Rev.* **2018**, *118*, 3447.
- [8] J. Hou, O. Inganas, R. H. Friend, F. Gao, *Nat. Mater.* **2018**, *17*, 119.
- [9] C. Yan, S. Barlow, Z. Wang, H. Yan, A. K. Y. Jen, S. R. Marder, X. Zhan, *Nat. Rev. Mater.* **2018**, *3*, 18003.
- [10] J. Guo, J. Min, *Adv. Energy Mater.* **2019**, *9*, 1802521.
- [11] A. Wadsworth, M. Moser, A. Marks, M. S. Little, N. Gasparini, C. J. Brabec, D. Baran, I. McCulloch, *Chem. Soc. Rev.* **2019**, *48*, 1596.
- [12] C. Sun, F. Pan, H. Bin, J. Zhang, L. Xue, B. Qiu, Z. Wei, Z. G. Zhang, Y. Li, *Nat. Commun.* **2018**, *9*, 743.
- [13] J. E. Yu, S. J. Jeon, J. Y. Choi, Y. W. Han, E. J. Ko, D. K. Moon, *Small* **2019**, *15*, 1805321.
- [14] S. J. Jeon, Y. W. Han, D. K. Moon, *Sol. RRL* **2019**, *3*, 1900094.
- [15] S. J. Jeon, Y. W. Han, D. K. Moon, *Small* **2019**, *15*, 1902598.
- [16] J. Lee, S. M. Lee, S. Chen, T. Kumari, S. H. Kang, Y. Cho, C. Yang, *Adv. Mater.* **2018**, *1*, 1804762.
- [17] H. Wu, H. Fan, S. Xu, L. Ye, Y. Guo, Y. Yi, H. Ade, X. Zhu, *Small* **2019**, *15*, 1804271.
- [18] X. Xue, K. Weng, F. Qi, Y. Zhang, Z. Wang, J. Ali, D. Wei, Y. Sun, F. Liu, M. Wan, J. Liu, L. Huo, *Adv. Energy Mater.* **2019**, *9*, 1802686.
- [19] H. B. Naveed, W. Ma, *Joule* **2018**, *2*, 621.
- [20] Y. Li, N. Zheng, L. Yu, S. Wen, C. Gao, M. Sun, R. Yang, *Adv. Mater.* **2019**, *31*, 1807832.
- [21] H. Hu, K. Jiang, P. C. Y. Chow, L. Ye, G. Zhang, Z. Li, J. H. Carpenter, H. Ade, H. Yan, *Adv. Energy Mater.* **2018**, *8*, 1701674.
- [22] S. J. Jeon, Y. W. Han, D. K. Moon, *ACS Appl. Mater. Interfaces* **2019**, *11*, 9239.
- [23] W. Zhao, S. Li, H. Yao, S. Zhang, Y. Zhang, B. Yang, J. Hou, *J. Am. Chem. Soc.* **2017**, *139*, 7148.
- [24] G. Li, Q. Xu, C. Chang, Q. Fan, X. Zhu, W. Li, X. Guo, M. Zhang, W. Y. Wong, *Macromol. Rapid Commun.* **2019**, *40*, 1800660.
- [25] C. Chang, W. Li, X. Guo, B. Guo, C. Ye, W. Su, Q. Fan, M. Zhang, *Org. Electron.* **2018**, *58*, 82.
- [26] J. Y. Kim, S. Park, S. Lee, H. Ahn, S. Y. Joe, B. J. Kim, H. J. Son, *Adv. Energy Mater.* **2018**, *8*, 1870132.
- [27] M. H. Hoang, G. E. Park, S. Choi, C. G. Park, S. H. Park, T. Van Nguyen, S. Kim, K. Kwak, M. J. Cho, D. H. Choi, *J. Mater. Chem. C* **2019**, *7*, 111.
- [28] S. Li, L. Zhan, C. Sun, H. Zhu, G. Zhou, W. Yang, M. Shi, C. Z. Li, J. Hou, Y. Li, H. Chen, *J. Am. Chem. Soc.* **2019**, *141*, 3073.
- [29] H. Cha, C. H. Tan, J. Wu, Y. Dong, W. Zhang, H. Chen, S. Rajaram, K. S. Narayan, I. McCulloch, J. R. Durrant, *Adv. Energy Mater.* **2018**, *8*, 1801537.
- [30] Z. Zhang, W. Liu, T. Rehman, H. X. Ju, J. Mai, X. Lu, M. Shi, J. Zhu, C. Z. Li, H. Chen, *J. Mater. Chem. A* **2017**, *5*, 9649.
- [31] Z. Zheng, O. M. Awartani, B. Gautam, D. Liu, Y. Qin, W. Li, A. Bataller, K. Gundogdu, H. Ade, J. Hou, *Adv. Mater.* **2017**, *29*, 1604241.
- [32] Z. He, C. Zhong, S. Su, M. Xu, H. Wu, Y. Cao, *Nat. Photonics* **2012**, *6*, 591.
- [33] Z. Li, K. Jiang, G. Yang, J. Y. L. Lai, T. Ma, J. Zhao, W. Ma, H. Yan, *Nat. Commun.* **2016**, *7*, 13094.
- [34] G. E. Park, S. Choi, S. Y. Park, D. H. Lee, M. J. Cho, D. H. Choi, *Adv. Energy Mater.* **2017**, *7*, 1700566.
- [35] S. Holliday, R. S. Ashraf, A. Wadsworth, D. Baran, S. A. Yousaf, C. B. Nielsen, C. H. Tan, S. D. Dimitrov, Z. Shang, N. Gasparini, M. Alamoudi, F. Laquai, C. J. Brabec, A. Salleo, J. R. Durrant, I. McCulloch, *Nat. Commun.* **2016**, *7*, 11585.
- [36] D. Baran, R. S. Ashraf, D. A. Hanifi, M. Abdelsamie, N. Gasparini, J. A. Röhr, S. Holliday, A. Wadsworth, S. Lockett, M. Neophytou, C. J. M. Emmott, J. Nelson, C. J. Brabec, A. Amassian, A. Salleo, T. Kirchartz, J. R. Durrant, I. McCulloch, *Nat. Mater.* **2017**, *16*, 363.
- [37] N. Li, J. D. Perea, T. Kassar, M. Richter, T. Heumueller, G. J. Matt, Y. Hou, N. S. Güldal, H. Chen, S. Chen, S. Langner, M. Berlinghof, T. Unruh, C. J. Brabec, *Nat. Commun.* **2017**, *8*, 14541.
- [38] J. Kong, S. Song, M. Yoo, G. Y. Lee, O. Kwon, J. K. Park, H. Back, G. Kim, S. H. Lee, H. Suh, K. Lee, *Nat. Commun.* **2014**, *5*, 5688.
- [39] P. Cheng, X. Zhan, *Chem. Soc. Rev.* **2016**, *45*, 2544.
- [40] L. Ying, F. Huang, G. C. Bazan, *Nat. Commun.* **2017**, *8*, 14047.
- [41] G. Zhang, X. Xu, Z. Bi, W. Ma, D. Tang, Y. Li, Q. Peng, *Adv. Funct. Mater.* **2018**, *28*, 1706404.
- [42] M. Saito, T. Koganezawa, I. Osaka, *ACS Appl. Mater. Interfaces* **2018**, *10*, 32420.
- [43] L. Ye, W. Li, X. Guo, M. Zhang, H. Ade, *Chem. Mater.* **2019**, *31*, 6568.

- [44] B. Qiu, S. Chen, H. Li, Z. Luo, J. Yao, C. Sun, X. Li, L. Xue, Z.-G. Zhang, C. Yang, Y. Li, *Chem. Mater.* **2019**, *31*, 6558.
- [45] H. Zhou, L. Yang, A. C. Stuart, S. C. Price, S. Liu, W. You, *Angew. Chem., Int. Ed.* **2011**, *50*, 2995.
- [46] X. Liu, B. Xie, C. Duan, Z. Wang, B. Fan, K. Zhang, B. Lin, F. J. M. Colberts, W. Ma, R. A. J. Janssen, F. Huang, Y. Cao, *J. Mater. Chem. A* **2018**, *6*, 395.
- [47] R. Xue, J. Zhang, Y. Li, Y. Li, *Small* **2018**, *14*, 1801793.
- [48] Y. Lin, F. Zhao, Y. Wu, K. Chen, Y. Xia, G. Li, S. K. K. Prasad, J. Zhu, L. Huo, H. Bin, Z. G. Zhang, X. Guo, M. Zhang, Y. Sun, F. Gao, Z. Wei, W. Ma, C. Wang, J. Hodgkiss, Z. Bo, O. Inganäs, Y. Li, X. Zhan, *Adv. Mater.* **2017**, *29*, 1604155.
- [49] L. Ye, Y. Xie, K. Weng, H. S. Ryu, C. Li, Y. Cai, H. Fu, D. Wei, H. Y. Woo, S. Tan, Y. Sun, *Nano Energy* **2019**, *58*, 220.
- [50] Y. W. Han, S. J. Jeon, H. S. Lee, H. Park, K. S. Kim, H.-W. Lee, D. K. Moon, *Adv. Energy Mater.* **2019**, *9*, 1902065.
- [51] H. Bin, Y. Yang, Z.-G. Zhang, L. Ye, M. Ghasemi, S. Chen, Y. Zhang, C. Zhang, C. Sun, L. Xue, C. Yang, H. Ade, Y. Li, *J. Am. Chem. Soc.* **2017**, *139*, 5085.
- [52] J. Liu, L.-K. Ma, Z. Li, H. Hu, T. Ma, C. Zhu, H. Ade, H. Yan, *J. Mater. Chem. A* **2017**, *5*, 22480.
- [53] Q. Li, L.-M. Wang, S. Liu, X. Zhang, T. Zhu, Z. Cao, H. Lai, J. Zhao, Y. Cai, W. Xie, F. Huang, *ACS Appl. Mater. Interfaces* **2019**, *11*, 45979.
- [54] S. M. Lee, T. Kumari, B. Lee, Y. Cho, J. Lee, J. Oh, M. Jeon, S. Jung, C. Yang, *Small* **2020**, *16*, 1905309.
- [55] X. Yi, Z. Peng, B. Xu, D. Seyitliyev, C. H. Y. Ho, E. O. Danilov, T. Kim, J. R. Reynolds, A. Amassian, K. Gundogdu, H. Ade, F. So, *Adv. Energy Mater.* **2020**, 1902430.
- [56] L. Lu, T. Zheng, Q. Wu, A. M. Schneider, D. Zhao, L. Yu, *Chem. Rev.* **2015**, *115*, 12666.
- [57] G. P. Kini, S. J. Jeon, D. K. Moon, *Adv. Mater.* **2020**, 1906175.